Advanced Powder Technology 28 (2017) 1309–1315

Contents lists available at ScienceDirect

Advanced Powder Technology

journal homepage: www.elsevier.com/locate/apt

Original Research Paper

Exploration of structural, thermal, vibrational and spectroscopic properties of new noncentrosymmetric double borate $Rb_3NdB_6O_{12}$

V.V. Atuchin [a,b,c,d,e,*], A.K. Subanakov [f], A.S. Aleksandrovsky [g,h], B.G. Bazarov [f], J.G. Bazarova [f], S.G. Dorzhieva [f], T.A. Gavrilova [i], A.S. Krylov [j], M.S. Molokeev [k,l,m], A.S. Oreshonkov [j,n], A.M. Pugachev [o], Yu.L. Tushinova [f], A.P. Yelisseyev [p]

[a] Laboratory of Optical Materials and Structures, Institute of Semiconductor Physics, SB RAS, Novosibirsk 630090, Russia
[b] Functional Electronics Laboratory, Tomsk State University, Tomsk 634050, Russia
[c] Laboratory of Semiconductor and Dielectric Materials, Novosibirsk State University, Novosibirsk 630090, Russia
[d] Institute of Chemistry, Tyumen State University, Tyumen 525003, Russia
[e] Laboratory of Single Crystal Growth, South Ural State University, Chelyabinsk 454080, Russia
[f] Laboratory of Oxide Systems, Baikal Institute of Nature Management, SB RAS, Ulan-Ude 670047, Russia
[g] Laboratory of Coherent Optics, Kirensky Institute of Physics, Federal Research Center KSC SB RAS, Krasnoyarsk 660036, Russia
[h] Laboratory for Nonlinear Optics and Spectroscopy, Siberian Federal University, Krasnoyarsk 660041, Russia
[i] Laboratory of Nanodiagnostics and Nanolithography, Institute of Semiconductor Physics, SB RAS, Novosibirsk 630090, Russia
[j] Laboratory of Molecular Spectroscopy, Kirensky Institute of Physics, Federal Research Center KSC SB RAS, Krasnoyarsk 660036, Russia
[k] Laboratory of Crystal Physics, Kirensky Institute of Physics, Federal Research Center KSC SB RAS, Krasnoyarsk 660036, Russia
[l] Department of Physics, Far Eastern State Transport University, Khabarovsk 680021, Russia
[m] Siberian Federal University, Krasnoyarsk 660041, Russia
[n] Department of Photonics and Laser Technologies, Siberian Federal University, Krasnoyarsk 660079, Russia
[o] Laboratory of Condensed Matter Spectroscopy, Institute of Automation and Electrometry, SB RAS, Novosibirsk 630090, Russia
[p] Laboratory of High Pressure Minerals and Diamond Deposits, Institute of Geology and Mineralogy, SB RAS, Novosibirsk 630090, Russia

ARTICLE INFO

Article history:
Received 12 September 2016
Received in revised form 4 February 2017
Accepted 16 February 2017
Available online 28 February 2017

Keywords:
Rubidium neodymium borate
Solid state reaction
Rietveld refinement
DSC
Raman scattering

ABSTRACT

New noncentrosymmetric rare earth borate $Rb_3NdB_6O_{12}$ is found in the ternary system Rb_2O–Nd_2O_3–B_2O_3. The $Rb_3NdB_6O_{12}$ powder was fabricated by solid state synthesis at 1050 K for 72 h and the crystal structure was obtained by the Rietveld method. $Rb_3NdB_6O_{12}$ crystallized in space group $R32$ with unit cell parameters $a = 13.5236(4)$, $c = 31.162(1)$ Å, $Z = 3$. From DSC measurements, the reversible phase transition (I type) in $Rb_3NdB_6O_{12}$ is observed at 852–936 K. The 200 μm thick tablet is transparent over the spectral range of 0.3–6.5 μm and the band gap is found as $E_g \sim 6.29$ eV. Nonlinear optical response of $Rb_3NdB_6O_{12}$ tested via SHG is estimated to be higher than that of $K_3YB_6O_{12}$. Blue shift of Nd luminescent lines is found in comparison with other borates. The vibrational parameters of $Rb_3NdB_6O_{12}$ are evaluated by experimental methods.

1. Introduction

Over the recent years, borate crystals have attracted great attention of researchers because of their high chemical stability, wide transparency range and appropriate nonlinear optical properties [1–10]. Recently, continuously tunable nonlinear-optical generation across vacuum ultraviolet range down to the wavelength as short as 121 nm was obtained in one of borates [11], this wavelength being the shortest one at which the coherent radiation was ever obtained in the solid state. The boron atom ability to exist in the three- and four-fold coordinations defines a large diversity of possible anion radicals in borate structures. The variety of existing and possible structural arrays of borates is continuously enriched by newly discovered compounds with higher performance characteristics. One borate subset, rare earth borates, is unique as the crystals that may exhibit laser properties through the luminescent rare earth centers and nonlinear optical (NLO) properties through the borate anionic framework simultaneously in a single compound. For example, $RCa_4O(BO_3)_3$ (R = La, Nd, Sm, Gd, Er and Y) [12], $YAl_3(BO_3)_4$(YAB) [13] and $Na_3La_9O_3(BO_3)_8$ [14] are nonlinear

* Corresponding author at: Institute of Semiconductor Physics, Novosibirsk 630090, Russia. Fax: +7 (383) 3332771.
E-mail address: atuchin@isp.nsc.ru (V.V. Atuchin).

http://dx.doi.org/10.1016/j.apt.2017.02.019

optical (NLO) and self-frequency doubling (SFD) materials, ytterbium doped $Li_6Y(BO_3)_3$ can be used in short pulse laser applications [15], $(Y,Gd)BO_3:Eu^{3+}$ is used as the red phosphor material in plasma display panels (PDP) [16] and $Li_6M_{1-x}Ce_x(BO_3)_3$ (M = Y, Gd) may be used as thermal neutron detectors [17].

In $M_2O–RE_2O_3–B_2O_3$ (M = alkali metal, RE = rare earth or Y) systems, only several noncentrosymmetric compounds have been found, namely $Na_3La_2(BO_3)_3$ [18], $Na_3La_9O_3(BO_3)_8$ [19], $Rb_3Y_2(BO_3)_3$ [20], $K_3YB_6O_{12}$ [21,22], $K_{21}Y_8B_{45}O_{90}$ [23] and $K_3TbB_6O_{12}$ [24]. This indicates that the ternary systems are complex and that different noncentrosymmetric structures can formed in the borate compounds. As for compasition $K_3YB_6O_{12}$, this double borate crystallizes in the trigonal space group $R32$ (a = 13.2202(19), c = 30.281 (6) Å, Z = 15), possesses a noticeable SHG signal and UV cut-off edge - as short as 195 nm [21]. Comparatively, another structure was recently found in $K_3TbB_6O_{12}$ [24], which crystallizes in the space group $R32$ (a = 13.2310 (12), c = 15.2490 (16) Å, Z = 9). The partial K/Tb disordering was elucidated in this structure. However, it should be mentioned that the $K_3YB_6O_{12}$ structure can be obtained from the $K_3TbB_6O_{12}$ structure by the emergence of instability at (0, 0, 3/2) k_8-point (T) of Brillouin zone. Thus, the existence of the phase transition on cooling could be assumed, when the high-temperature parent $K_3TbB_6O_{12}$ structure transforms to the low-temperature ordered $K_3YB_6O_{12}$ structure. As it appears, borates with larger alkali metal ions are most promising for searching new nonlinear optical materials because the ions are more susceptible to polarization and may contribute to the overall NLO response. It should be pointed, that optical characteristics of $Rb_3Y_2B_3O_9$ remain unknown [20]. The present study is aimed at the synthesis and comparative exploration of physical properties of a new $Rb_3NdB_6O_{12}$ compound formed in system $Rb_2O–Nd_2O_3–B_2O_3$.

2. Experimental

The samples were prepared by solid state reactions using high-purity starting reagents (Red Chemist, Ltd., Russia): Rb_2CO_3 (99.9%), Nd_2O_3 (99.99%), and H_3BO_3 (99.99%). Before weighing, Rb_2CO_3 was preheated at 900 °C for 24 h to remove any absorbed water. The reagents were weighed on an analytical balance with the accuracy of 0.1 mg. The mixtures of Rb_2CO_3, Nd_2O_3 and H_3BO_3 in stoichiometric proportions were thoroughly ground in an agate mortar, slowly heated in a muffle furnace to 500 °C at the rate of 1 °C/min and held at this temperature for 24 h. Then, the samples had been reground and annealed at 700–750 °C for 24–72 h until equilibrium was reached. Temperatures were measured with a Pt–PtRh thermocouple. The temperature was controlled to be within ±2 °C up to 1200 °C with an OMRON controller. After the heat treatment, the sample was slowly cooled to room temperature together with the furnace and the estimated cooling rate was ~12 °C/min. The equilibrium was specified when two successive heat treatments resulted in the identical X-ray patterns.

The powder X-ray diffraction data were recorded by a D8 ADVANCE Bruker AXS diffractometer (Vantec-1 detector) at room temperature using CuK_α radiation and scanning over the range of 2θ = 8–100°. The step size of 2θ was 0.021° and the counting time was 10 s per step. The Rietveld refinement was implemented using TOPAS 4.2 [25]. Almost all peaks were indexed by a trigonal cell (space group $R32$) with the parameters close to those of $K_3YB_6O_{12}$ [21].

Differential scanning calorimetric (DSC) measurements were performed on a STA 449 F1 Jupiter thermoanalyzer (NETZSCH) over the temperature range of 30–900 °C in the argon flow. Pt crucibles were used as vessels. Pt–PtRh thermocouples were used for measurement. The precision of temperature measurement was ±1 °C. The heating and cooling rates were 10 °C/min. The second harmonic generation (SHG) response of powder samples was measured with a Q-switched YAG:Nd laser at λ_ω = 1064 nm, in the reflection mode. The SHG signal intensities ($I_{2\omega}$) from the sample and from the reference sample (polycrystalline α-SiO_2) were registered comparatively. The experimental setup configuration and sample preparation methods can be found elsewhere [26,27]. The absorption spectra in the mid-infrared (mIR) spectra were carried out to specify the boron coordination in the new compounds. The mIR spectra were obtained at room temperature using a Nicolet-380 infrared spectrophotometer with KBr pellets as standards. The spectra were obtained in the range from 500 to 2000 cm^{-1} with the resolution of 1 cm^{-1}. The unpolarized Raman spectra were collected in a backscattering geometry using a triple monochromator Horiba Jobin Yvon T64000 Raman spectrometer operating in the double subtractive mode and then detected by an LN-cooled charge-coupled device. The spectral resolution for the recorded Stokes side Raman spectra was set to ~4 cm^{-1} (this resolution was reached by using gratings with 1800 grooves/mm and 100 mm slits). The microscope system based on Olympus BX41 microscope with an Olympus 50^x objective lens f = 0.8 mm with numerical aperture NA = 0.75 provides a focal spot diameter of about 2 μm on the sample [28–30]. Single-mode argon 514.5 nm from a Spectra-Physics Stabilite 2017 Ar^+ laser of 5 mW on the sample was used as an excitation light source. The laser light intensity was adjusted to avoid the sample's heating.

3. Results and discussions

The synthesized product was a free-flowing powder of light lilac tint, as evident in Fig. 1, that is a characteristic of Nd-containing oxides. A typical SEM image of the particle is shown in Fig. 2. Thus, the synthesis resulted in the agglomerates 2–10 μm in size formed by strongly coalescent individual grains with a diameter below 1 μm. This micromorphology is common when the temperature/-time conditions selected for synthesis are high enough for the active oxide grain interdiffusion [7,31–33]. It should be pointed that the particles possess strong charging effect during SEM measurements and this indicates their very low conductivity common for the oxides without oxygen vacancies. The initial examination of the XRD pattern of the synthesized compound revealed that it

Fig. 1. The photo image of $Rb_3NdB_6O_{12}$ powder on the grey background, as illuminated by white light.

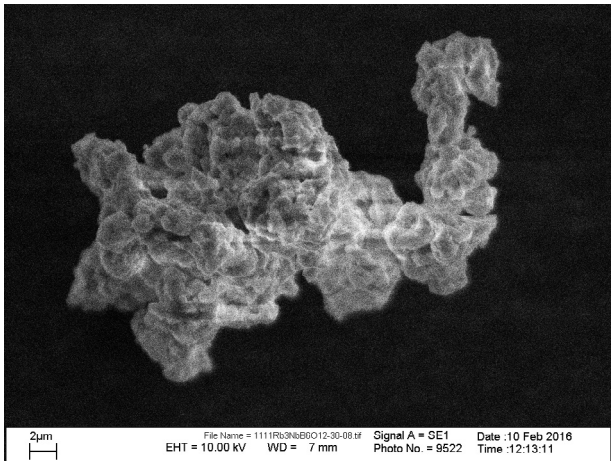

Fig. 2. SEM pattern of the $Rb_3NdB_6O_{12}$ particle.

resembles that of $K_3YB_6O_{12}$. Therefore, the initial structure model and atomic positions of $K_3YB_6O_{12}$ were adopted as a starting point of the structure refinement. The final Rietveld profiles are shown in Fig. 3. There are no foreign diffraction peaks in the pattern. $Rb_3NdB_6O_{12}$ crystallizes in the non-centrosymmetric space group *R*32, as it was supported by SHG measurements. The SHG intensity from $Rb_3NdB_6O_{12}$ powder was four times higher than that of reference α-SiO_2 sample. It should be mentioned, however, that the SHG signal appeared under pumping at $\lambda_\omega = 1064$ nm is partly damped in $Rb_3NdB_6O_{12}$ because of a strong absorption band at ~530 nm. Thus, the real intensity of SHG effect in $Rb_3NdB_6O_{12}$ is the above-measured level and it is higher than that of $K_3YB_6O_{12}$ [21]. The weak SHG effect of $K_3YB_6O_{12}$ is due to the B_5O_{10} groups which are aligned in the almost opposite directions and, consequently, they contribute little to the SHG effect. Therefore, it is likely that the introduction of rare earth ion, like Nd, instead of Y, partially violates the compensation of nonlinear optical response in the system of B_5O_{10} groups, or nonlinear optical polarizability of the $Rb_3NdB_6O_{12}$ unit cell is higher than that of $K_3YB_6O_{12}$ due to a higher contribution of Nd-O complexes than that of Y-O complexes. The structure refinement was stable and gives low *R*-factors (Table 1). The atom coordinates and the main bond lengths are given in Table 2 and Table 1S, respectively. Further details of the crystal structure may be obtained from Fachinformationszentrum Karlsruhe, 76344 Eggenstein-Leopoldshafen, Germany (fax: (+49)7247-808-666; E-mail: crystdata@fiz-karlsruhe.de; http://www.fiz-karlsruhe.de/request_for_deposited_data.html on quoting the deposition number: CSD-431936.

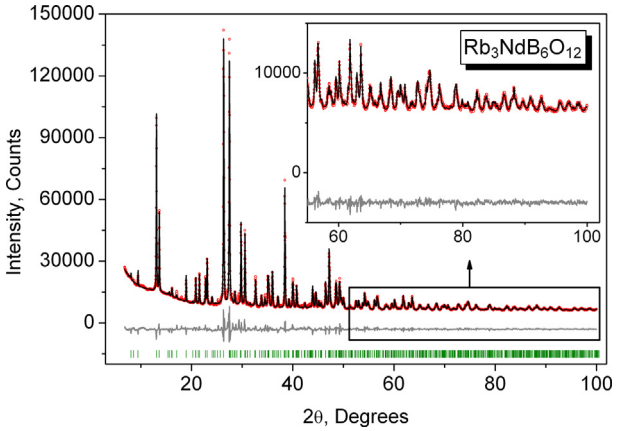

Fig. 3. The measured (red), calculated (black) and differential (grey) diffraction patterns of $Rb_3NdB_6O_{12}$. (For interpretation of the references to colour in this figure legend, the reader is referred to the web version of this article.)

Table 1
Main parameters of processing and refinement of $Rb_3NdB_6O_{12}$.

Compound	$Rb_3NdB_6O_{12}$
Space group	*R*32
a, Å	13.5236 (4)
c, Å	31.162 (1)
V, Å^3	4935.6 (3)
Z	3
2θ-interval, °	5–100
No. of reflections	671
No. of refined parameters	112
R_{wp}, %	4.58
R_p, %	3.09
R_{exp}, %	0.96
χ^2	4.75
R_B, %	1.75

Table 2
Fractional atomic coordinates and isotropic displacement parameters (Å^2) of $Rb_3NdB_6O_{12}$.

	x	*y*	*z*	B_{iso}
$Rb_3NdB_6O_{12}$				
Nd1	1/3	2/3	−0.2159 (5)	0.9 (6)
Nd2	1/3	2/3	−0.7195 (5)	0.5 (5)
Nd3	1/3	2/3	2/3	2.0 (9)
Rb1	0.124 (2)	1/3	5/6	2.0 (5)
Rb2	2/3	0.795 (2)	1/3	2.0 (5)
Rb3	0.185 (1)	0.855 (1)	−0.4186 (6)	2.0 (4)
Rb4	1/3	2/3	−0.5797 (9)	1.9 (5)
Rb5	1/3	2/3	1/6	2.0 (5)
B1	0.19 (2)	0.78 (2)	−0.278 (6)	2 (1)
B2	0.20 (3)	0.77 (3)	−0.515 (5)	2 (1)
B3	0.46 (3)	0.89 (2)	−0.650 (5)	2 (1)
B4	0.67 (3)	1.08 (2)	−0.419 (7)	2 (1)
B5	0.47 (3)	0.92 (1)	−0.892 (6)	2 (1)
O1	0.27 (1)	0.774 (9)	−0.483 (2)	1.5 (6)
O2	0.169 (7)	0.567 (9)	−0.681 (2)	1.5 (6)
O3	0.390 (7)	0.808 (5)	−0.389 (2)	1.5 (6)
O4	0.283 (7)	0.774 (5)	−0.768 (2)	1.5 (6)
O5	0.517 (7)	0.857 (8)	−0.620 (3)	1.5 (6)
O6	0.522 (8)	0.855 (7)	−0.541 (3)	1.5 (6)
O7	0.495 (6)	1.009 (6)	−0.647 (2)	1.5 (6)
O8	0.668 (6)	0.806 (6)	−0.525 (2)	1.5 (6)
O9	0.594 (7)	1.04 (1)	−0.580 (3)	1.5 (6)
O10	0.097 (8)	0.729 (7)	−0.750 (3)	1.5 (6)

The $Rb_3NdB_6O_{12}$ structure contains a three-dimensional framework composed of $[B_5O_{10}]^{5-}$ groups bridged by Nd-O polyhedra (Fig. 4). The $[B_5O_{10}]^{5-}$ group consists of one BO_4 tetrahedron and four BO_3 triangles that form double B-O rings via the common tetrahedron (Fig. 4a). All the B-O rings in this structure can be divided into two groups, with one group approximately parallel and the other - perpendicular to the *c* axis. Each $[B_5O_{10}]^{5-}$ group is linked to four different Nd-O polyhedra and, likewise, each Nd-O polyhedron is connected to four neighboring $[B_5O_{10}]^{5-}$ groups. The Nd-O polyhedra are formed by the face-sharing linked NdO_6 octahedra. Rb^+ cations are located in large cavities of the framework structure (Fig. 4). It is interesting to compare the structural parameters of $K_3YB_6O_{12}$ [21] and $Rb_3NdB_6O_{12}$. When K^+ and Y^{3+} ions are substituted by bigger ions Rb^+ and Nd^{3+}, cell parameters *a* and *c* increase by 2.2 and 2.9%, respectively, and that results in the drastic unit cell volume increase by 7.7%. Because of the framework-type structure, the cell swelling is provided by nearly equally sized variations along different crystallographic directions. Thus, it could be reasonably assumed that the $K_3YB_6O_{12}$ type structure is very stable and the crystal family $A_3TB_6O_{12}$ (A = K, Rb; T = Y, rare earth) is abundant.

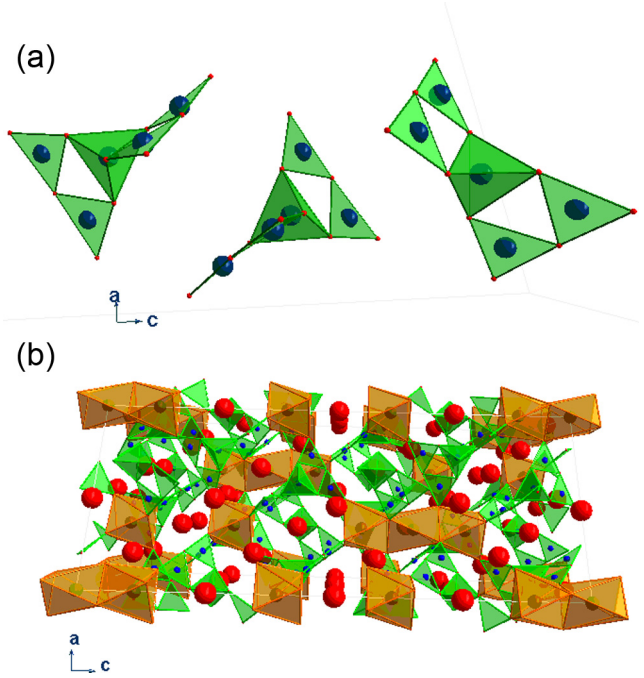

Fig. 4. The crystal structure of $Rb_3NdB_6O_{12}$: (a) view of the $[B_5O_{10}]^{5-}$ anionic groups, (b) the projection view along the *b*-axis.

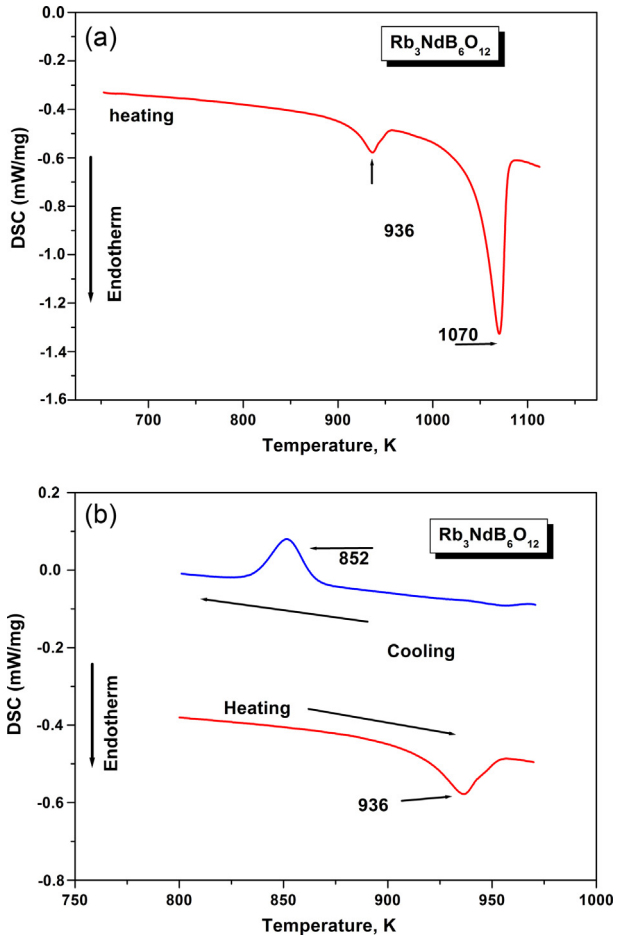

Fig. 5. DSC measurements: (a) heating up to melting and (b) heating-cooling over the temperature range of 298–813 K.

The DSC curves recorded from $Rb_3NdB_6O_{12}$ are shown in Fig. 5. Two endothermic signals at 936 and 1070 K were detected upon the sample heating, as shown in Fig. 5(a). The endothermic peak at 1070 K corresponds to the melting point of $Rb_3NdB_6O_{12}$. The X-ray diffraction measurements indicate the incongruent melting of the borate. To determine the nature of the endoeffect at 936 K, the other sample was recorded in the "heating-cooling" mode over the temperature range of 298–813 K (without melting). At cooling, $Rb_3NdB_6O_{12}$ shows an exothermic effect at 852 K. The obtained temperature hysteresis is as high as ~80 K. Thus, the signature observed at 852–936 K reveals the existence of a reversible phase transition (type I) in $Rb_3NdB_6O_{12}$ and, respectively, special experiments are topical to define the structure of the high-temperature modification of β-$Rb_3NdB_6O_{12}$ stable over the range of 936–1070 K. It should be pointed that the transition was not found in $K_3YB_6O_{12}$ [21]. Respectively, it can be reasonably assumed that the existence of the phase transition in the $A_3TB_6O_{12}$ (A = K, Rb; T = Y, rare earth) borates depends on the big cation combination.

The transmission spectrum recorded for the $Rb_3NdB_6O_{12}$ tablet is given in Fig. 6. One can see that the 200 μm thick tablet is transparent over the spectral range of 0.3–6.5 μm and there is an abundant set of sharp absorption bands. A gradual transparency increase on the wavelength increase in the UV and visible spectral ranges is associated with the Rayleigh light scattering on the grain boundaries in the powder. The fundamental absorption edge position is well detected as a step in the diffuse reflectance (DR) spectrum (Fig. 6, curve 2) or in the transmission spectra recorded for a mixture of KBr and $Rb_3NdB_6O_{12}$ powders (Fig. 6, curve 1). In the DR spectra, the band gap value is estimated, usually, from the midpoint of the slope in this step [34]. In $Rb_3NdB_6O_{12}$, the midpoint is located nearly 197 nm and it is marked by a star in curve 2. Thus, in this borate, the band gap is $E_g \sim 6.29$ eV. The analysis of the absorption edge shape shows a straightening in the coordinates $(\alpha \cdot h\nu)^2 = f(h\nu)$, where α is an absorption coefficient and $h\nu$ is the photon energy. This means that there is a direct allowed electronic transition between the parabolic bands. The Tauc plot is shown in Fig. 7 [35,36] and the band gap can be estimated from the cross-point between this straight line and the abscissa axis. The obtained band gap value is 6.25 eV at room temperature, which is very close to the value found from the DR spectrum. The observed band gap is very close to that of $K_3YB_6O_{12}$ [21]. That means that the replacement of Y by Nd does not lead to the red shift of fundamental absorption, and f-d transitions of the Nd ion in the structure under study are positioned below 200 nm. The intense absorption bands, evident in the transmission spectra shown in Fig. 6, should be attributed to the well-known optical transitions in Nd^{3+} ions [37]. These are electronic transitions from the $^4I_{9/2}$ ground state to different excited states. The transitions are given in Table 3 using the conventional nomenclature [37]. Here, the spectral position of the band is given in the left column and the corresponding excited state is depicted in the right column.

The photoluminescence spectrum (PL) recorded under the excitation at 325 nm is given in Fig. 8. Two groups of strong narrow lines in the range of 860–940 nm with components 873.9, 877.8, 884.3, 913.9, 931.4 nm and in the range of 1020–1100 nm (1052, 1086 nm) are observed in the PL spectrum. The most intense lines are underlined here. These two groups are associated with electronic transitions $^4F_{3/2} \rightarrow {}^4I_{9/2}$ and $^4F_{3/2} \rightarrow {}^4I_{11/2}$, respectively. Five luminescence lines of the first group evidently are due to the transitions from the lowest sublevel of the $^4F_{3/2}$ multiplet to five sublevels of the crystal field split $^4I_{9/2}$ ground state. Therefore, the positions of these sublevels at room temperature are 0, 50, 135, 501 and 706 cm^{-1}. This splitting is somehow smaller than that for the Nd ion in the YAG host. The position of the lowest sublevel of the $^4F_{3/2}$ multiplet is at 11443 cm^{-1}, being 20 cm^{-1} blue-shifted

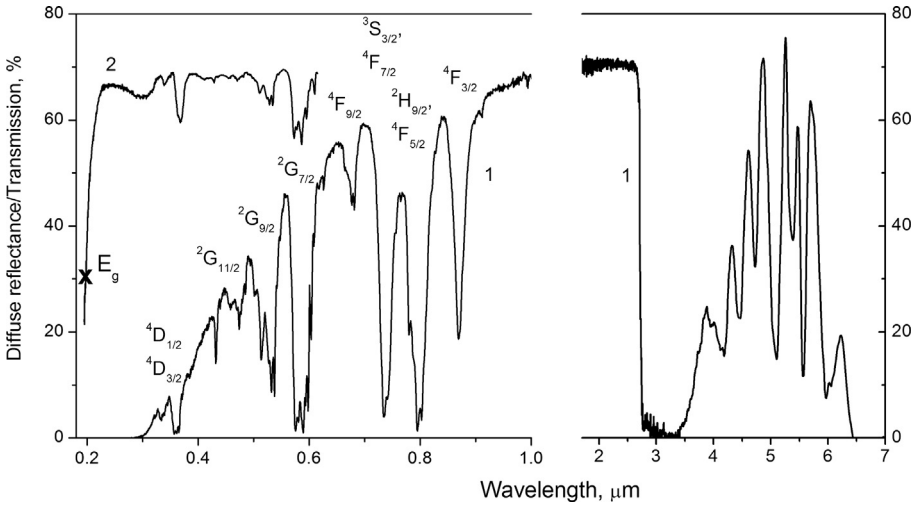

Fig. 6. Transmission (1, 2) and diffuse reflectance (3) spectra, as recorded for the $Rb_3NdB_6O_{12}$ powder (1, 3) and for the $KBr/Rb_3NdB_6O_{12}$ mixture (2) at $T = 300$ K.

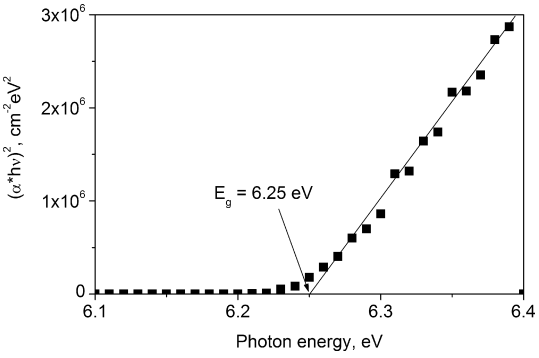

Fig. 7. The Tauc plot: The shape of the fundamental absorption edge represented in coordinates $(\alpha * h\nu)^2 = f(h\nu)$, for curve 1 in Fig. 6a. Here α is an absorption coefficient in (cm^{-1}) and $h\nu$ is photon energy. The bandgap is $E_g = 6.25$ eV.

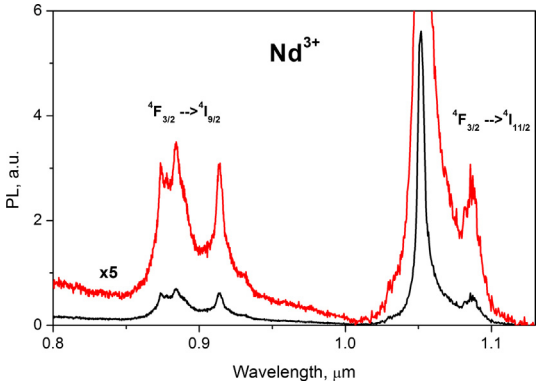

Fig. 8. Photoluminescence spectra of $Rb_3NdB_6O_{12}$ powder excited at 325 nm, at 300 K, are shown in black. The red curves correspond to the same spectra shown with the 5× multiplication. (For interpretation of the references to colour in this figure legend, the reader is referred to the web version of this article.)

Table 3
Absorption band maxima and Nd^{3+} excited states in$Rb_3NdB_6O_{12}$.

Absorption band maximum, nm	Excited state
361	$^4D_{1/2} + {}^4D_{3/2}$
456/474	$^2G_{11/2}$
514/630	$^2G_{9/2}$
575/587	$^2G_{7/2}$
679	$^4F_{9/2}$
735	$^3S_{3/2} + {}^4F_{7/2}$
800	$^2H_{9/2} + {}^4F_{5/2}$
867	$^4F_{3/2}$

with respect to that in YAG. Both of these features result in a considerable blue shift of the baricenter of luminescence $^4F_{3/2} \rightarrow {}^4I_{9/2}$ with respect to the Nd:YAG one. After the UV-visible light absorption, the Nd^{3+} ions relax nonradiatively via excited states to the lower excited state $^4F_{3/2}$. Further electronic transition to the ^4I_i multiplets of the ground state, where $i = 9/2$, 11/2, 13/2 and 15/2, occurs radiatively, with the near IR emission. The oxides doped with Nd are often used as active media for solid state lasers emitting near 1 μm. The position of the most intense line near 1052 nm is blue shifted with respect to that in Nd:YAG and it is very close to that in phosphate glass or in YLF fluoride laser crystal. It is interesting to note that the lasing wavelength of Nd in other borates' family, namely, in huntite-structured trigonal borates, is at 1060 nm and does not exhibit such strong blue shift like that found in the trigonal borate under study. This fact indicates the unique character of the influence of the host crystal matrix under investigation on Nd ions.

The Wyckoff positions of atoms, Raman and IR active vibrational modes of $Rb_3NdB_6O_{12}$ are shown in Table 4. The vibrational representation of the *R*32 phase at the Brillouin zone center is $53A_1 + 57A_2 + 110E$. The detail assignment of the internal vibrational modes in $Rb_3NdB_6O_{12}$ is rather difficult due to the structure complexity. The Raman and IR spectra can be described in the framework of $[B_5O_{10}]^{5-}$ groups, which consist of four BO_3 triangles and one BO_4 tetrahedron not independent from each other in the crystal. The lowering of the BO_3 and BO_4 groups symmetry may produce new allowed phonon modes which can appear both in Raman and in IR spectra. The Raman and IR spectra of $Rb_3NdB_6O_{12}$ are shown in Figs. 9 and 10, respectively. The three normal vibration modes of planar BO_3 triangles ν_2, ν_3, and ν_4, are infrared-active, and ν_1, ν_3, and ν_4 are Raman-active, all four normal vibrations of tetrahedral BO_4 groups are Raman-active, whereas only ν_3 and ν_4 are infrared-active [38]. Thus, according to [38], ν_1 non-degenerate B–O symmetric stretching vibrations are located in the range of 900–975 cm^{-1}, and they should be Raman-active only, as seen in Fig. 9. Out-of-plane bending vibrations ν_2 are positioned within the 700–800 cm^{-1} range and should be visible in IR spectra only [39], as evident from Fig. 10. However, the spectral lines related to ν_1 and ν_2 vibrations of BO_3 become activated both

Table 4
Wyckoff positions of atoms and vibrational modes in $Rb_3NdB_6O_{12}$.

Atom	Wyckoff position	Mechanical representation
Rb1	9e	$A_1 + 2A_2 + 3E$
Rb2	9d	$A_1 + 2A_2 + 3E$
Nd1, Nd2, Rb4	6c	$A_1 + A_2 + 2E$
Rb5	3b	$A_2 + E$
Nd3	3a	$A_2 + E$
Rb3, B1–B5, O1–O10	18f	$3A_1 + 3A_2 + 6E$
Total		$53A_1 + 57A_2 + 110E$
Acoustic		$A_2 + E$
Optic		$53A_1 + 56A_2 + 109E$
Raman active modes		$53A_1 + 109E$
IR active modes		$56A_2 + 109E$

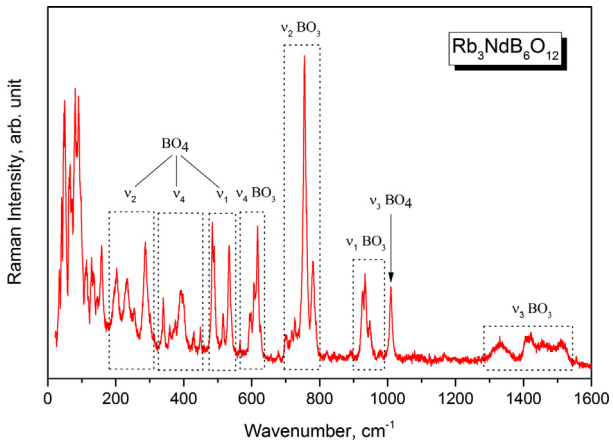

Fig. 9. The Raman spectrum of $Rb_3NdB_6O_{12}$.

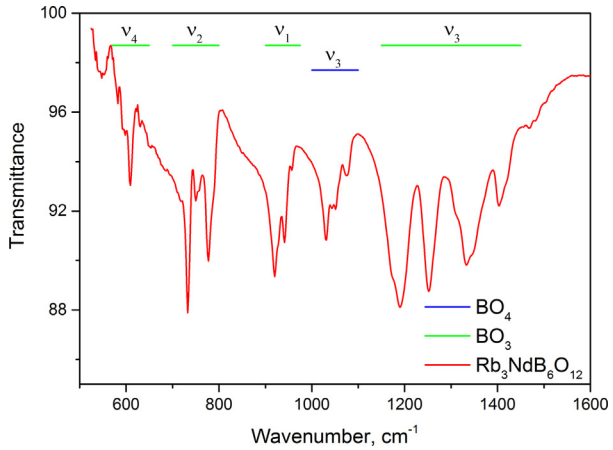

Fig. 10. The IR spectra of $Rb_3REB_6O_{12}$.

in Raman and in IR spectra due to lowering of the XY_3 planar group symmetry [40]. Several spectral lines associated with ν_3 vibrations should be positioned in vibrational spectra over the region of 1150–1200 cm^{-1} (Fig. 10) [41]. However, the Raman signals from $Rb_3NdB_6O_{12}$ in this region are very weak (Fig. 9). On the other hand, the Raman peaks related to ν_3 can be found in the range of 1300–1500 cm^{-1} [38,42]. Thus, we can assume that doubly degenerate antisymmetric B–O stretching vibrations ν_3 should be located in the regions of 1200–1500 cm^{-1}, being active in both Raman and IR spectra. Double-degenerate in-plane O–B–O bending vibration ν_4 should be located in the region of 570–650 cm^{-1} and is both Raman and infrared active, too. All four normal vibrations are Raman-active, whereas only ν_3 and ν_4 are infrared active in case of BO_4 groups. According to [38], ν_1 symmetric stretching mode of BO_4 should be located in the area of 500–540 cm^{-1} in Raman spectra only. The ν_2 bending vibrations must be found in the range of 200 cm^{-1}, ν_3 asymmetric stretching vibrations are positioned in the range of 1000–1100 cm^{-1} and the ν_4 bending mode in the range of 260–350 cm^{-1}. The remaining Raman and IR lines in the wavenumber region below 200 cm^{-1} are related to the rotational and translational vibrations of coupled $[B_5O_{10}]^{5-}$ groups.

In Fig. 1S, the luminescence spectra of $Rb_3NdB_6O_{12}$ and the well-known fluoride crystal NdF_3 are compared. Red line in Fig. 1S depicts the 514.5 nm-excited luminescence of the Nd ion in $Rb_3NdB_6O_{12}$. The reference crystal (NdF_3) luminescence is presented in blue for comparison. A shorter-wavelength part of $Rb_3NdB_6O_{12}$ spectrum contains the Raman contribution. The rest of $Rb_3NdB_6O_{12}$ spectrum, in contrast to the spectrum of the reference fluoride crystal, shows almost complete absence of the luminescence from higher excited states, except for a weak luminescent band around 800 nm. This band originates from superposed $^4F_{5/2}$ and $^2H_{9/2}$ states. The strong luminescence in the vicinity of 900 nm is due to the $^4F_{3/2} \rightarrow {}^4I_{9/2}$ transition. This result evidences strong relaxation from upper excited levels to $^4F_{3/2}$ in $Rb_3NdB_6O_{12}$. The influence of radiativeless relaxation on the population of the $^4F_{3/2}$ level in $Rb_3NdB_6O_{12}$ is much smaller than that of higher excited levels; however, for laser applications, the use of diluted crystals, e.g., $Rb_3(Gd_{1-x}Nd_x)B_6O_{12}$ would be desirable.

4. Conclusions

The new noncentrosymmetric double borate $Rb_3NdB_6O_{12}$ was synthesized by the solid state reaction method and its crystal structure was obtained in noncentrosymmetric space group *R*32 by the Rietveld analysis. The structure features a three-dimensional framework composed of $[B_5O_{10}]^{5-}$ groups that are bridged by Nd-O polyhedra. The spectroscopic properties of $Rb_3NdB_6O_{12}$ are evaluated in detail. The wideband optical transmission and the appropriate SHG signal are observed in this compound. On the base of the crystal chemistry analysis, it can be reasonably assumed that the $K_3YB_6O_{12}$ type structure is very stable and, respectively, the borate family $A_3TB_6O_{12}$ (A = K, Rb; T = Y, rare earth) is abundant. In this case, the $A_3TB_6O_{12}$ family is promising for the design of phosphors containing different rare elements in T^{3+} state or their combination. Besides, if the crystal growth of $A_3TB_6O_{12}$ borates will be successful, they can be considered as new self-activated nonlinear optical materials promising for application in laser technology. Thus, it is topical to search for new nonlinear optical trigonal borates from the $A_3TB_6O_{12}$ family.

Acknowledgements

We are grateful to Guochun Zhang for the crystal structure data on $K_3YB_6O_{12}$, and O. Tsydenova and A. Sarapulova for her consultations. This research was supported by SB RAS Program No.II.2P (No. 0356-2015-0412) and RSF (14-22-0143). The reported study was funded by RFBR according to the research projects 15-02-04950 and 15-52-53080, 16-32-00351, 16-52-48010 and 17-52-53031. Also, the work was supported by Act 211 Government of the Russian Federation, contract 02.A03.21.0011 and by the Ministry of Education and Science of the Russian Federation (4.1346.2017/PP).

Appendix A. Supplementary material

Supplementary data associated with this article can be found, in the online version, at http://dx.doi.org/10.1016/j.apt.2017.02.019.

References

[1] Y. Mori, Y.K. Yap, T. Kamimura, M. Yoshimura, T. Sasaki, Recent development of nonlinear borate crystals for UV generation, Opt. Mater. 19 (2002) 1–5.

[2] C. Chen, Z. Lin, Z. Wang, The development of new borate-based UV nonlinear optical crystals, Appl. Phys. B 80 (2005) 1–25.

[3] V.V. Atuchin, L.D. Pokrovsky, V.G. Kesler, L.I. Isaenko, L.I. Gubenko, Structure and chemistry of LiB_3O_5 (LBO) optical surfaces, J. Ceram. Proc. Res. 4 (2003) 84–87.

[4] A.P. Vasilenko, A.V. Kolesnikov, E.M. Trukhanov, N.A. Pylneva, A.M. Yurkin, V.V. Atuchin, X-ray topography study of LiB_3O_5 crystals grown from molybdate flux, J. Phys.: Condens. Matter 15 (2003) 6801–6808.

[5] V.V. Atuchin, L.D. Pokrovsky, V.G. Kesler, N.Yu. Maklakova, M. Yoshimura, N. Ushiyama, T. Matsui, K. Kamimura, Y. Mori, T. Sasaki, Cesium accumulation at CsB_3O_5 optical surface, Opt. Mater. 23 (2003) 377–383.

[6] A.S. Aleksandrovsky, A.M. Vyunishev, I.E. Shakhura, A.I. Zaitsev, A.V. Zamkov, Random quasi-phase-matching in a nonlinear photonic crystal structure of strontium tetraborate, Phys. Rev. A 78 (2008) 031802.

[7] V.V. Atuchin, B.G. Bazarov, T.A. Gavrilova, V.G. Grossman, M.S. Molokeev, Zh.G. Bazarova, Preparation and structural properties of nonlinear optical borates $K_{2(1-x)}Rb_{2x}Al_2B_2O_7$, $0 < x < 0.75$, J. Alloys Compd. 515 (25) (2012) 119–122.

[8] R.V. Kurbatov, L.A. Solovyov, B.G. Bazarov, A.K. Subanakov, J.G. Bazarova, Synthesis, structure and properties of $RbMgBO_3$, Solid State Commun. 172 (2013) 33–36.

[9] V.V. Atuchin, S.V. Adichtchev, B.G. Bazarov, Zh.G. Bazarova, T.A. Gavrilova, V.G. Grossman, V.G. Kesler, G.S. Meng, Z.S. Lin, N.V. Surovtsev, Electronic structure and vibrational properties of $KRbAl_2B_2O_7$, Mater. Res. Bull. 48 (3) (2013) 929–934.

[10] A.I. Zaitsev, A.S. Aleksandrovsky, A.S. Kozhukhov, L.D. Pokrovsky, V.V. Atuchin, Growth, optical and microstructural properties of PbB_4O_7 plate crystals, Opt. Mater. 37 (2014) 298–301.

[11] P. Trabs, F. Noack, A.S. Aleksandrovsky, A.I. Zaitsev, V. Petrov, Generation of coherent radiation in the vacuum UV using randomly quasi-phase-matched strontium tetraborate, Opt. Lett. 41 (2016) 618–621.

[12] R. Norrestam, M. Nygren, J.O. Bovin, Structural investigations of new calcium-rare earth (R) oxyborates with the composition $Ca_4RO(BO_3)_3$, Chem. Mater. 4 (1992) 737–743.

[13] A.D. Mills, Crystallographic data for new rare earth borate compounds, $RX_3(BO_3)_4$, Inorg. Chem. 1 (1962) 960–961.

[14] P. Gravereau, J.-P. Chaminade, S. Pechev, V. Nikolov, P. Peshev, $Na_3La_9O_3(BO_3)_8$, a new oxyborate in the ternary system Na_2O-La_2O_3-B_2O_3: preparation and crystal structure, Solid State Sci. 4 (2002) 993–998.

[15] J. Sablayrolles, V. Jubera, J.P. Chaminade, I. Manek-Honninger, S. Murugan, T. Cardinal, R. Olazcuaga, A. Garcia, F. Salin, Crystal growth, luminescent and lasing properties of the ytterbium doped $Li_6Y(BO_3)_3$ compound, Opt. Mater. 27 (2005) 1681–1685.

[16] G. Chadeyron, R. Mahiou, M. EL-Ghozzi, A. Arbus, D. Zambon, J.C. Cousseins, Luminescence of the orthoborate YBO_3: Eu^{3+}. Relationship with crystal structure, J. Lumin. 72–74 (1997) 564–566.

[17] J.P. Chaminade, O. Viraphong, F. Guillen, C. Fouassier, B. Czirr, Crystal growth and optical properties of new neutron detectors Ce^{3+}: $Li_6R(BO_3)_3$ (R = Gd, Y), IEEE T. Nucl. Sci. 48 (2001) 1158–1161.

[18] Z.H. Li, J.H. Zeng, G.C. Zhang, Y.D. Li, A new promising phosphor, $Na_3La_2(BO_3)_3$: Ln (Ln = Eu, Tb), J. Solid State Chem. 178 (2005) 3624–3630.

[19] J.X. Zhang, G.L. Wang, Z.L. Liu, L.R. Wang, G.C. Zhang, X. Zhang, Y. Wu, P.Z. Fu, Y. C. Wu, Growth and optical properties of a new nonlinear $Na_3La_9O_3(BO_3)_8$ crystal, Opt. Exp. 18 (1) (2010) 237–243.

[20] J.H. Gao, R.K. Li, $Rb_3Y_2(BO_3)_3$ with a noncentrosymmetric structure, Acta Crystallogr. C 63 (2007) i112–i114.

[21] S.G. Zhao, G.C. Zhang, J.Y. Yao, Y.C. Wu, $K_3YB_6O_{12}$: a new nonlinear optical crystal with a short UV cutoff edge, Mater. Res. Bull. 47 (11) (2012) 3810–3813.

[22] Li Yang, Yingpeng Wan, Honggen Weng, Yanlin Huang, Cuili Chen, Hyo Jin Seo, Luminescence and color center distributions in $K_3YB_6O_{12}$:Ce^{3+} phosphor, J. Phys. D: Appl. Phys. 49 (32) (2016) 325303.

[23] Kai Feng, Wenlong Yin, Wenyu Hao, Jiyong Yao, Yicheng Wu, A novel UV nonlinear optical crystal material: $K_{21}Yb_8B_{45}O_{90}$, CrystEngComm 15 (25) (2013) 5064–5069.

[24] Dan Zhao, Fa-Xue Ma, Rui-Juan Zhang, Min Huang, Peng-Fei Chen, Rong-Hua Zhang, Wei Wei, Substitution disorder and photoluminescent property of a new rare-earth borate: $K_3TbB_6O_{12}$, Z. Kristallogr. 231 (9) (2016) 525–530.

[25] Bruker AXS TOPAS V4: General profile and structure analysis software for powder diffraction data. User's Manual. Bruker AXS, Karlsruhe, Germany, 2008.

[26] E.V. Alekseev, O. Felbinger, S.J. Wu, T. Malcherek, W. Depmeier, G. Modolo, T.M. Gesing, S.V. Krivovichev, E.V. Suleimanov, T.A. Gavrilova, L.D. Pokrovsky, A.M. Pugachev, N.V. Surovtsev, V.V. Atuchin, $K[AsW_2O_9]$, the first member of the arsenate-tungsten bronze family: synthesis, structure, spectroscopic and non-linear optical properties, J. Solid State Chem. 204 (2013) 59–63.

[27] P. Zhao, M. Mangir Murshed, E.V. Alekseev, V.V. Atuchin, A.M. Pugachev, T.M. Gesing, Synthesis, structure and properties of $Na[AsW_2O_9]$, Mater. Res. Bull. 60 (2014) e258–e263.

[28] A.S. Aleksandrovsky, I.A. Gudim, A.S. Krylov, V.L. Temerov, Luminescence of yttrium aluminum borate single crystals doped with manganese, Phys. Solid State 49 (9) (2007) 1695–1699.

[29] V.V. Atuchin, A.S. Aleksandrovsky, O.D. Chimitova, T.A. Gavrilova, A.S. Krylov, M.S. Molokeev, A.S. Oreshonkov, B.G. Bazarov, J.G. Bazarova, Synthesis and spectroscopic properties of monoclinic α-$Eu_2(MoO_4)_3$, J. Phys. Chem. C 118 (2014) 15404–15411.

[30] A.S. Oreshonkov, A.K. Khodzhibaev, A.S. Krylov, M.F. Umarov, A.N. Vtyurin, Raman spectroscopy study of the behavior of the soft mode in a structural phase transition in the $Pr_3Sb_5O_{12}$ crystal, Phys. Solid State 57 (2015) 2286–2289.

[31] V.V. Atuchin, T.A. Gavrilova, J.-C. Grivel, V.G. Kesler, Electronic structure of layered titanate $Nd_2Ti_2O_7$, Surf. Sci. 602 (2008) 3095–3099.

[32] V.V. Atuchin, V.G. Grossman, S.V. Adichtchev, N.V. Surovtsev, T.A. Gavrilova, B. G. Bazarov, Structural and vibrational properties of microcrystalline $TlM(MoO_4)_2$ (M = Nd, Pr) molybdates, Opt. Mater. 34 (2012) 812–816.

[33] Chang Sung Lim, Victor V. Atuchin, Aleksandr S. Aleksandrovsky, Maxim S. Molokeev, Preparation of $NaSrLa(WO_4)_3$:Ho^{3+}/Yb^{3+} ternary tungstates and their upconversion photoluminescence properties, Mater. Lett. 181 (2016) 38–41.

[34] M. Nowak, B. Kauch, P. Szperlich, Determination of energy band gap of nanocrystalline SbSI using diffuse reflectance spectroscopy, Rev. Sci. Instrum. 80 (2009) 046107.

[35] J. Tauc, Optical properties and electronic structure of amorphous Ge and Si, Mater. Res. Bull. 3 (1968) 37–46.

[36] D. Errandonea, A. Muñoz, P. Rodríguez-Hernández, J.E. Proctor, F. Sapiña, M. Bettinelli, Theoretical and experimental study of the crystal structures, lattice vibrations, and band structures of monazite type $PbCrO_4$, $PbSeO_4$, $SrCrO_4$, and $SrSeO_4$, Inorg. Chem. 54 (15) (2015) 7524–7535.

[37] D.T. Sviridov, R.K. Sviridova, Yu.F. Smirnov, Optical Spectra of Transition Metals in Crystals, Nauka, Moscow, 1976.

[38] K. Nakamoto, Infrared and Raman Spectra of Inorganic and Coordination Compounds, sixth ed., Wiley, New York, 2009.

[39] S.Z. Shmurak, V.V. Kedrov, A.P. Kiselev, T.N. Fursova, I.M. Shmyt'ko, Spectral and structural features of $Lu_{1-x}RE_xBO_3$ compounds, Phys. Solid State 57 (8) (2015) 1588–1600.

[40] Ji. Zhang, Renqin Dou, Deming Zhang, Qingli Zhang, Shaotang Yin, Structure, Raman and infrared spectroscopic properties of new nonlinear optical material $Na_3VO_2B_6O_{11}$, J. Mol. Struct. 1118 (2016) 378–382.

[41] Xianshun Lv, Yuguo Yang, Bing Liu, Yuanyuan Zhang, Lei Wei, Xian Zhao, Xuping Wang, Electronic structure and Raman spectroscopy study of dibarium magnesium orthophosphate, $Ba_2Mg(BO_3)_2$, Vib. Spectr. 80 (2015) 53–58.

[42] X.B. Xu, J.Y. Wang, C.Q. Zhang, X.G. Xu, Raman study of phonons in $K_2Al_2B_2O_7$ crystals, Appl. Phys. Lett. 85 (12) (2004) 2241–2243.